

Playing for 3D Human Recovery

Zhongang Cai^{*,1,2}, Mingyuan Zhang^{*,1}, Jiawei Ren^{*,1}, Chen Wei¹, Daxuan Ren^{1,2}, Jiatong Li^{1,2}
 Zhengyu Lin², Haiyu Zhao², Shuai Yi², Lei Yang², Chen Change Loy¹, Ziwei Liu¹
¹S-Lab, Nanyang Technological University ²SenseTime Research

<https://gta-human.com>

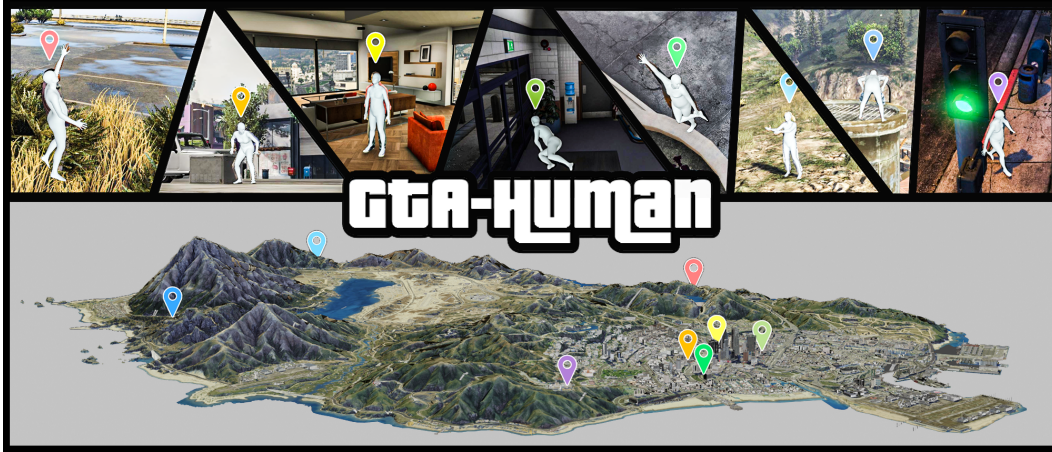


Figure 1. **GTA-Human dataset** is built from GTA-V, an open-world action game that features a reasonably realistic functioning metropolis and virtual characters living in it. Our customized toolchain enables large-scale collection and annotation of highly diverse human data (subjects, actions, locations) that we hope empowers in-depth studies on 3D human recovery. We show here a few examples we generate at various locations in the virtual world with our SMPL annotations overlaid on them.

Abstract

Image- and video-based 3D human recovery (i.e. pose and shape estimation) have achieved substantial progress. However, due to the prohibitive cost of motion capture, existing datasets are often limited in scale and diversity, which hinders the further development of more powerful models. In this work, we obtain massive human sequences as well as their 3D ground truths by playing video games. Specifically, we contribute, **GTA-Human**, a mega-scale and highly-diverse 3D human dataset generated with the GTA-V game engine. With a rich set of subjects, actions, and scenarios, **GTA-Human** serves as both an effective training source. Notably, the “unreasonable effectiveness of data” phenomenon is validated in 3D human recovery using our game-playing data. A simple frame-based baseline trained on **GTA-Human** already outperforms more sophisticated methods by a large margin; for video-based methods, **GTA-Human** demonstrates superiority over even the in-domain training set. We extend our study to larger models to observe the same consistent improvements, and the study on supervision signals suggests the rich collection of SMPL

annotations is key. Furthermore, equipped with the diverse annotations in **GTA-Human**, we systematically investigate the performance of various methods under a wide spectrum of real-world variations, e.g. camera angles, poses, and occlusions. We hope our work could pave way for scaling up 3D human recovery to the real world.

1. Introduction

Image- and video-based 3D human recovery, i.e. simultaneous estimation of human pose and shape via parametric models such as SMPL [38], have transformed the landscape of holistic human understanding. This technology is critical for entertainment, gaming, augmented and virtual reality industries. However, despite that the exciting surge of deep learning is arguably driven by enormous labelled data [31, 58], there is yet a similar effort to revolutionize this field. The insufficiency of data is attributed to the prohibitive cost of 3D parametric model annotations [53]. Existing datasets are either small in scale [33, 56, 63], lacking diversity [18, 22, 65], or not providing the 3D parametric model

annotation at all [1, 19, 20, 36].

To address the aforementioned limitations of existing datasets for human pose and shape estimation, we present **GTA-Human**, a mega-scale dataset with rich annotations and diverse scenarios. GTA-Human is built from a customized pipeline to generate data with the popular video game Grand Theft Auto V (referred to as GTA-V), which empowers an immersive experience in a reasonably realistic open world around a metropolis. To allow investigation into the impact of the amount of data, GTA-Human consists of 1.4 million SMPL parametric labels in 20K video sequences. GTA-Human also has several appealing properties as an ideal data source for 3D human recovery, and allows for systematic study on multiple factors that are otherwise difficult to evaluate in real life. **1) Diverse Subjects:** With more than 600 subjects of different gender, age, ethnicity, body shape and clothing, GTA-Human provides a wide coverage of human appearances. **2) Rich Actions:** We sample 20,000 actions from an in-game database of daily human activities that is huge enough to assign each video sequence a unique action. **3) Extensive Scenarios:** GTA-Human has a rich collection of scenes captured in drastically different locations of six major categories from city streets to the wild. **4) Camera Angles** are manipulated in each sequence to reflect a realistic distribution. **5) Subject-environment interaction** that give rises to occlusion of various extents. **6) Time of the day** that affects lighting conditions, and **weather system** that mimics the real climate changes. GTA-Human is a comprehensive and challenging benchmark that supplements existing datasets for the further development of 3D human recovery.

Equipped with GTA-Human, we conduct experiments to gain the following valuable insights for the 3D human recovery task. **1) The unreasonable effectiveness of data.** We show that given sufficient data, HMR [23], one of the first deep learning-based methods for SMPL estimation with relatively simplistic architecture, is able to outperform recent works with more sophisticated designs or additional information such as SPIN [28] and VIBE [26]. Consistent improvements are observed with various practical settings, such as blended training with real data and pretraining followed by finetuning. In addition, our experiments on video-based method VIBE [26] give even more exciting results: an equal amount of synthetic GTA-Human data is as good as real-captured indoor dataset; the full set of GTA-Human is surprisingly on par with in-domain training data, showcasing the power of the large amount of decent-quality data. **2) Big data and big models.** Despite recent development in deeper convolutional networks [14, 64] and vision transformers [8, 60] in computer vision research, the model size remains unchanged for 3D human recovery [23, 26, 28]. We extend our study to deeper CNNs and recently developed transformers, and validate big models can be trained with GTA-Human to yield

consistent improvements. **3) Strong supervision (SMPL) is crucial.** Compared to previous large-scale human pose estimation benchmarks that only provide 3D keypoints, we demonstrate that strong supervision in the form of SMPL parameters is important for training a strong model. This observation also reaffirms the value of GTA-Human as an effective training source that provides nearly free and highly scalable SMPL annotations. **4) Our full-spectrum analysis identifies factors that are critical to 3D human recovery.** Our systematic investigation on camera angles, occlusions, pose distributions, and lighting conditions offer important insights to develop better 3D human models.

2. Related Work

Real Datasets. Motion capture facilities are built to achieve high-accuracy 3D annotations. HumanEva [56] and Human3.6M [18] utilize optical motion capture systems, but intrusive markers are needed to be placed on the subjects. Total Capture [61] MuPoTS-3D [42], Panoptic Studio [22], and HUMBI [65] make use of multiple camera views and require no intrusive marker. However, the background is constant and thus lacking diversity. 3DPW [63] combines IMU and a moving camera to build an in-the-wild dataset with 3D annotations. Unfortunately, the IMU drift is still an obstacle and the dataset only contains a small number of videos. SMPLy [33] constructs point clouds from multi-view capture of “frozen” people and fits SMPL on them. However, the scale of the dataset is limited by the difficulty of collecting videos that meet the special setup requirement.

Synthetic or Mixed Datasets. SURREAL [62], Hoffmann *et al.* [15] render textured SMPL body models in real-image backgrounds. However, this strategy neglects the fact that the geometry of the clothes is unaccounted for by SMPL, and the mismatch results in unrealistic subjects. 3DPeople [50] uses clothed human models while MPI-INF-3DHP [40] takes segmented subjects from images and paste them onto new backgrounds in the training set. But the subject-background interaction is still unnatural. AGORA [46] is the latest synthetic dataset featuring high-quality annotations by rendering real human scans in a virtual world. However, the dataset is image-based and does not support the training of video-based methods. Richter *et al.* [51, 52], Krähenbühl *et al.* [30], JTA [9], GTA-IM [5] and SAIL-VOS 3D [16] have shown the possibilities of obtaining nearly free yet accurate annotations from video games. However, these datasets do not provide SMPL annotation needed for our investigation. We take inspirations from these works in building our GTA-Human.

3. GTA-Human Dataset

A rigorous comparison between GTA-Human and existing dataset is shown in Table 1. GTA-Human features 1.4 million individual SMPL annotations, the scale of which

Table 1. **3D Human dataset comparisons.** We compare GTA-Human with existing real datasets with SMPL annotations and synthetic datasets with highly realistic setups. GTA-Human features large scale and diversity. Datasets are divided into three types: R (real), S (synthetic) and M (mixed). ITW: in-the-wild. #SMPL: number of individual SMPL annotations. #Seq.: number of video sequences. #Subj.: number of subjects. #Act.: number of actions. GTA-Human has a large action dataset to sample from that allows a unique action to be assigned to each video sequence. Note that EFT [21] re-annotates 2D human pose estimation datasets where the number of subjects are difficult to trace. *: 3DPW and Panoptic Studio only have general descriptions of scene activities.

Dataset	Year	Type	ITW	Video	#SMPL	#Seq.	#Subj.	#Act.
HumanEva [56]	2009	R	-	✓	NA	7	4	6
Human3.6M [18]	2013	R	-	✓	312K	839	11	15
MPI-INF-3DHP [40]	2017	M	✓	✓	96K	16	8	8
3DPW [63]	2018	R	✓	✓	32K	60	18	*
Panoptic Studio [22]	2019	R	-	✓	736K	480	~100	*
EFT [21]	2020	R	✓	-	129K	NA	Many	NA
SMPLy [33]	2020	R	✓	✓	24K	567	742	NA
AGORA [46]	2021	S	✓	-	173K	NA	>350	NA
GTA-Human	2021	S	✓	✓	1.4M	20K	>600	20K

is the largest compared to other real datasets or synthetic datasets with realistic setups. Moreover, GTA-Human consists of in-the-wild scenes that are impossible to achieve in real life with complicated facilities, since motion capture systems are immobile and even require an indoor environment. In addition, GTA-Human provides video sequences instead of static images, supporting the research on video-based human recovery.

Inspired by existing works that uses GTA-generated data for various vision tasks [5, 9, 16, 30, 51, 52], our toolchain extracts ground truth 2D and 3D keypoints, semantic and depth maps from the game engine, followed by fitting SMPL models on the keypoints with temporal constraints. However, annotating 1.4 millions sets of SMPL parameters is far from trivial: we design and deploy an automatic system based on cloud services that scale to a large number of coordinated gaming and computational nodes. The technical details are included in the Supplementary Material.

3.1. Diverse Data Generation

Due to the immense difficulty and prohibitive cost of data collection and SMPL annotation for the 3D human recovery task, most existing datasets are built at restrictive locations such as indoor studios or laboratory environments. Furthermore, only a small number of subjects are employed to perform a limited set of actions. In contrast, GTA-Human is carefully designed to maximize the variety in the following aspects.

- **Subject.** GTA-Human collects over 600 subjects of different genders, ages, ethnic groups, clothing and body shapes for a wide coverage of human appearances. A selected set of the subjects are shown in Figure 2. We argue that the study on virtual humans is not only resource-friendly,

but also raises fewer privacy concerns. In addition, synthetic data has another desirable advantage. Unlike optical motion capture systems in real life that rely on intrusive markers to be placed on the subjects, accurate skeletal keypoints can be synthesized to eradicate unexpected visual cues of the markers and allow more clothing options.

- **Action.** Existing datasets either design a small number of actions [18, 40, 56], or lack a clearly defined action set [22, 63]. In contrast, we gain access to a large database of motion clips (actions) that can be used to manipulate the virtual characters. These actions provide an extremely holistic representation of city-dwellers’ daily activities, and are remarkably realistic because they are produced via motion capture of real human actors or actresses. We show several pose sequences and a visualization of their distribution in the Supplementary Material, with a more in-depth investigation of the impact of actions on human recovery in Section 4.5. We select 20,000 most dynamic and expressive actions, based on the pose sequence distribution, to provide a wide range of poses in GTA-Human.
- **Location.** The conventional optical [18, 56] or multi-view motion capture systems [22] require indoor environments, resulting in the scarcity of in-the-wild scenarios. Thanks to the open-world design of GTA, players have seamless access to various locations with diverse backgrounds. We categorize representative locations into *city, suburb, desert, forest, coast and indoor* (Figure 2). The subjects are naturally blended into the scenes thanks to the modern game engine, in contrast to existing works that crop and paste subjects onto random backgrounds [40, 62].
- **Interaction.** A significant advantage of GTA-Human is *the realistic subject-environment interaction* empowered by the physics engine that introduces wide varieties. We



Figure 2. **Data diversity in GTA-Human.** (a) GTA-Human contains more than 600 subjects of different genders, ages, ethnic groups, clothing and body shapes. (b) locations with various backgrounds are divided into six categorizes. (c) Realistic weather further enhances diversity. (d) In-game time are set to capture diverse lighting conditions. Note the shadow direction is affected by the sun position.

consider occlusion as a prominent example: subjects move behind structures (*e.g.* fences), vegetation (*e.g.* bushes), and other road users (*e.g.* other pedestrians and cars), making part of the body invisible from the camera. We capture occlusion by annotating if the body joints are occluded, and assign self-occlusion a separate label for convenient evaluation in Section 4.5. Other examples include the subject falling off the edge of a high platform, and the subject walking into a pond which causes water ripples. We include more interesting examples in the supplementary materials.

- **Camera Angle.** Recent studies [4] have shown the enormous impact of camera angles on model performance, yet its effect in 3D human recovery is under-explored due to the unavailability of such a dataset. It is common to have datasets with fixed camera positions [18, 22, 40, 56], where the only variation comes from the relative positions of the

camera and the subjects. In GTA-Human, we choose to sample *random camera positions from the distribution of the real datasets* (details are found in the Supplementary Material) to balance both diversity and realism. Section 4.5 presents our study on the camera angle.

- **Lighting and Weather.** A common data augmentation technique is by adjusting image exposure to mimic different lighting. As shown in Figure 2, we directly control the in-game time to *sample data round the clock*. Consequently, GTA-Human contains drastically different lighting conditions and shadow projections. In addition, we further introduce *random weather conditions such as rain and snow to the scenes* that would be otherwise difficult, if not impossible, to capture in real life. We show multiple sample images in Figure 2.

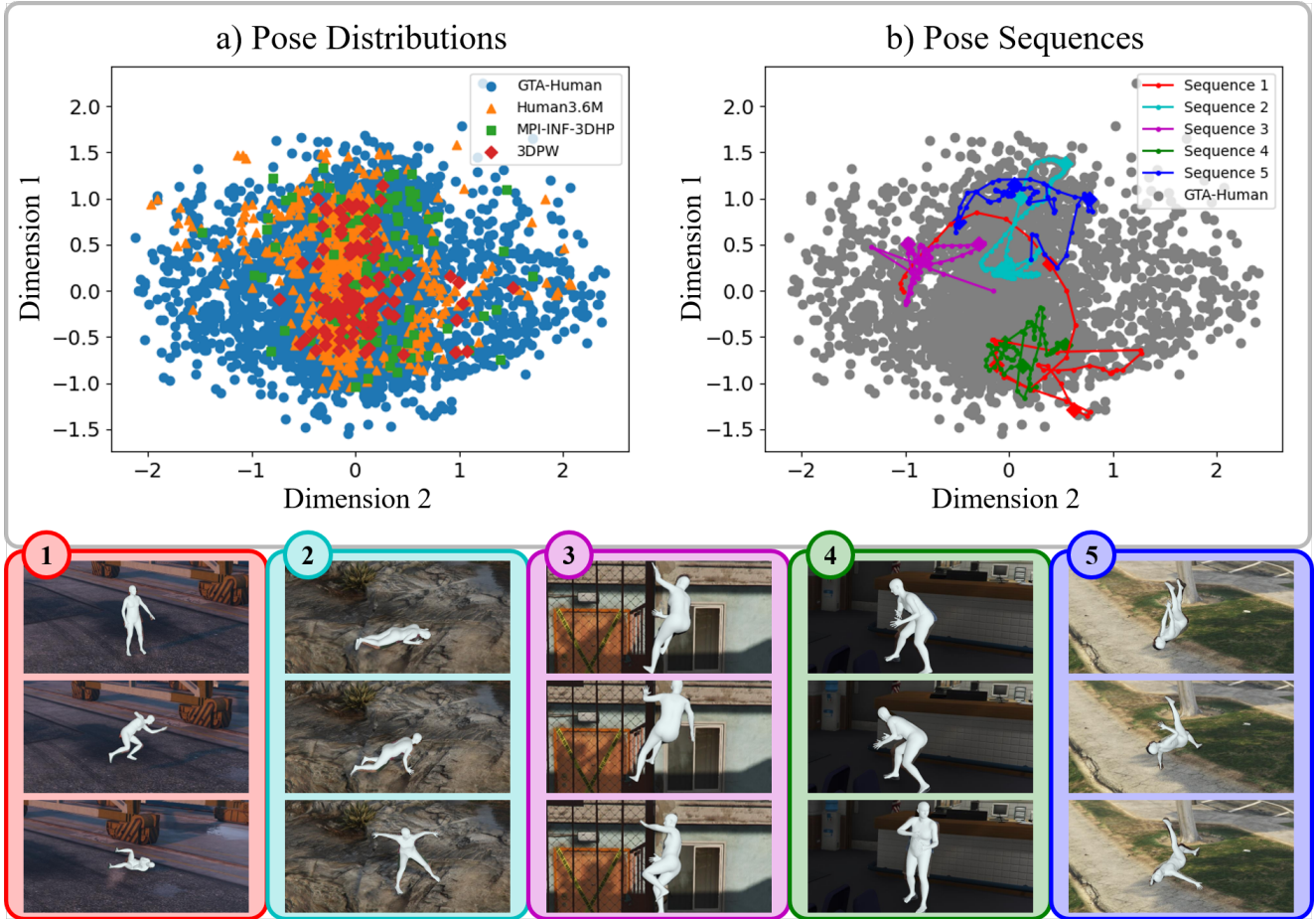


Figure 3. **Actions.** GTA-Human contains 20K actions that are expressive and diverse. (a) The distribution of poses in GTA-Human and real datasets are visualized after PCA dimension reduction. The distribution of GTA-Human poses does not only have the largest range, but also covers existing poses in the real datasets. (b) We show five pose sequences, represented by curves with each pose frame as the nodes. The same dimension reduction transformation as that in (a) is used. Representative frames of sequence 1-5 are visualized, which are indicated by the diamond-shaped nodes in (b). For visualization purpose of a), we randomly downsample data points from each datasets.

4. Experiments

We adopt HMR [23] with ResNet-50 backbone as the baseline for its popularity and simplicity. We also follow the convention to evaluate models on 3DPW [63] test set. The standard metrics are Mean Per Joint Position Error (MPJPE), and Procrustes-aligned [11] Mean Per Joint Position Error (PA-MPJPE), *i.e.*, MPJPE evaluated after rigid alignment of the predicted and the ground truth joint keypoints, both in millimeters (*mm*). We highlight that PA-MPJPE is the primary metric, on which we base most of our discussions. More details are included in the Supplementary Material.

4.1. The Unreasonable Effectiveness of Data

Image-based 3D Human Recovery. The experiments indicate adding massive data is extremely effective, which allows a baseline method to easily outperform more sophisticated counterparts (Table 2). We first build an improved version of HMR by including the MoSh [37] annotation of

Human3.6M in the training, following SPIN [28]. We empirically find that, despite the unavoidable reality gap, it is still possible to leverage a large amount of decent-quality synthetic data to boost performance. The method HMR-Mix represents adding synthetic GTA-Human data in the training, which achieves 5.7 mm further improvement in PA-MPJPE, surpassing methods such as SPIN [28] that requires online registration (resulting in very slow training) or VIBE [26] that leverages temporal information from videos. Besides utilizing synthetic data in the training, we also follow the strategy in AGORA [46] and apply synthetic data to fine-tune a trained SPIN model (whose network architecture is essentially the same as HMR), for which significant improvements are also achieved. It demonstrates the universal effectiveness of GTA-Human.

In Figure 4, we delve deeper into the impact of data quantity, and observe a consistent downward trend in the errors with increasing GTA-Human data used in the training.

Table 2. **The unreasonable effectiveness of data.** The values are reported on 3DPW [63] test set. The sheer amount of data of GTA-Human boosts the HMR baseline to outperform much more sophisticated methods such as SPIN that leverages online optimization (Opt) and VIBE that utilizes temporal information (Video). +: we train a strong HMR by including the MoSh [37] annotation of Human3.6M dataset in alignment with SPIN [28]. We employ two strategies: HMR-Mix that directly blends GTA-Human data with real data without any dataset weights applied; HMR-FT that follows AGORA [46] that evaluates the power of synthetic data by finetuning a pretrained a HMR model following the online registration proposed by SPIN. Huge performance improvements are achieved with both settings. We also conduct further experiments on video-based human recovery in Table 3. Real: real datasets. Blended: directly mixing GTA-Human data with real datasets, without using any dataset weights.

Method	Opt	Video	Pretrain	Train	Finetune	MPJPE ↓	PA-MPJPE ↓
HMR [23]	-	-	ImageNet	Real	-	130.0	76.7
HMR [23]+	-	-	ImageNet	Real	-	98.5	61.7
SPIN [28]	✓	-	ImageNet	Real	-	96.9	59.2
VIBE [26]	-	✓	ImageNet	Real	-	93.5	56.5
HMR-Mix	-	-	ImageNet	Blended	-	88.7	56.0
HMR-FT	-	-	SPIN	-	Blended	87.0	52.7

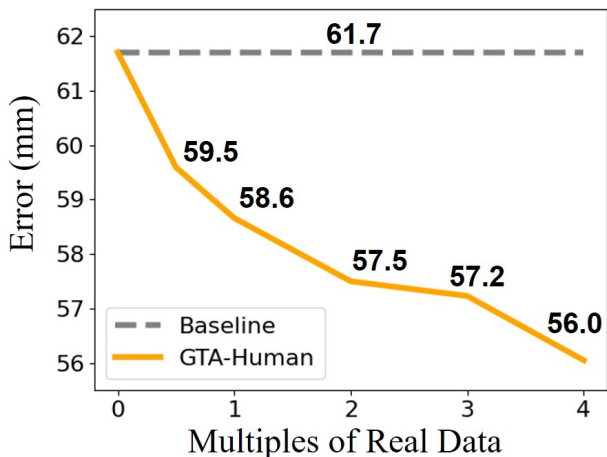


Figure 4. **Model performance against the amount of GTA-Human data**, expressed as multiples of data in the real datasets (~300K [28]). The evaluation metric is PA-MPJPE. A steady improvement is observed as an increasing amount of synthetic data is added.

We point out that no domain adaptation techniques have been applied in the training, indicating that GTA-Human is highly realistic and the sheer amount of data is effective.

Video-based 3D Human Recovery. We validate that similar boosts are also gained to video-based methods in Table 3, where VIBE [26] is used as the base model. We follow VIBE to use a trained SPIN model as the feature extractor for each frame, and train the temporal modules with datasets indicated in Table 3. **1)** Notably, GTA-Human even outperforms in-domain data, that is, a model trained on GTA-Human performs better on 3DPW test set than a model trained on the 3DPW train set itself. We attribute this unexpected result to the large scale of GTA-Human that is

about two orders of magnitude larger. This result is inspiring: neural networks can learn meaningful knowledge from synthetic data and transfer it to real scenarios. **2)** Moreover, we discover that the domain gap between indoor and outdoor data may be as significant as that between real and synthetic data. GTA-Human outperforms MPI-INF-3DHP, which is collected indoor, with the equal number of training data. GTA-Human is also complementary to all other video-based datasets; blending them together in the training achieves the best results.

4.2. Comparison with Data-driven Methods

We highlight that GTA-Human is a large-scale, decent-quality dataset for 3D human recovery. In Table 4, we compare GTA-Human with several other recent works that provide additional data for human pose and shape estimation. We show that GTA-Human is an effective training source that improves the performance of various base methods. Surprisingly, GTA-Human slightly outperforms AGORA, which leverages expensive real human scans of very high quality, indicating that a large amount of decent-quality data may just be as effective.

4.3. Big Data and Big Model

ResNet-50 remains the default backbone choice, since HMR [23] is firstly proposed for deep learning-based 3D human recovery. In this section, we extend our study of the impact of big data on more backbone options, including deeper CNNs such as ResNet-101 and 152 [14], as well as DeiT [60], one of the latest work in vision transformers. In Table 5, we replace the feature extractor of the HMR baseline with backbones that consist of a various number of parameters. As expected, the larger models demonstrate better capabilities. We highlight that the inclusion of GTA-Human always improves model performance, regardless of

Table 3. **The unreasonable effectiveness of data on video-based methods.** The values are reported on 3DPW [63] test set. We adopt VIBE [26] as the base model (whose per-frame feature extractor is a trained SPIN with parameters frozen) and use different datasets to train the temporal module. GTA-Human outperforms MPI-INF-3DHP which is collected indoor. The full set of GTA-Human is comparable with in-domain training source (3DPW train set), highlighting the power of a large amount of data. Blending other real datasets with GTA-Human leads to the best results. †: in-domain training data as the evaluation is conducted on 3DPW test set. *: downsampled GTA-Human data to match the size of MPI-INF-3DHP (96K SMPL poses). Accel: acceleration error for motion smoothness evaluation (mm/s^2).

MPI-INF-3DHP	3DPW†	GTA-Human	MPJPE ↓	PA-MPJPE ↓	Accel ↓
✓	-	-	95.0	56.5	27.1
-	✓	-	87.9	54.7	23.2
-	-	✓*	93.7	55.0	26.3
-	-	✓	91.3	54.1	24.7
-	✓	✓	85.2	52.4	24.2
✓	✓	✓	86.0	51.9	23.3

Table 4. **Comparison with other data-driven methods.** The results demonstrates the power of large-scale, high-quality GTA-Human data that significantly improves the base method performance. The numbers are obtained on 3DPW [63] test set, *without* using 3DPW in the training. †: HMR as the base method. ‡: SPIN as the base method. We consider HMR-FT uses SPIN as the base method as it leverages SPIN’s online registration in the pretraining stage. +#SMPL: number of additional SMPL annotations.

Dataset	+#SMPL	PA-MPJPE ↓
Arnab <i>et al.</i> [2] †	3M	72.2
EFT [21] ‡	129K	54.2
AGORA [46] ‡	173K	55.3
GTA-Human (HMR-Mix) †	1.4M	56.0
GTA-Human (HMR-FT) ‡	1.4M	52.7

the model size or architecture. Note that using transformers as the backbone for human pose and shape estimation is under-explored in recent literature. There is plenty of room for further improvement upon our attempts presented here. Nevertheless, the results are aligned with our conclusion that the effectiveness of big data is universal.

4.4. Strong Supervision is Key

We compare weak supervision signals (*i.e.* 2D and 3D keypoints) to strong counterparts (*i.e.* SMPL parameters), and find out that the latter is critical for high-performing regression-based models. We experiment under the blended training setting. Table 6 shows that strong supervision of SMPL parameters θ and β , are much more effective than weak supervision of body keypoints. In addition, HMR+ achieves more than 10 mm improvements in PA-MPJPE by simply including SMPL annotations via MoSh [37] in Table 2. This further exemplifies the effectiveness of the strong supervision signal. These observations may be attributed to the fact that strong supervision initiates gradient flow that

reaches the learnable SMPL parameters in the shortest possible route. More discussion is found in the Supplementary Material.

4.5. Systematic Study on Real-World Variations

Camera Angles. We confirm that the long-tailed distribution of camera angles leads to imbalanced model performance. We plot the model performance against camera angles in Figure 5(a-b). It is observed that the performance is closely related to the distribution density of training data. In particular, for elevation where the real data distribution concentrates around a small range of positive angles (camera is higher than the subject’s waist and slightly looking down), extreme angle causes the performance to degrade drastically. This observation suggests camera angle is a key factor to human pose and shape estimation. For real-life applications, our findings suggest that collecting data with similar camera positions to the use case would lead to better results.

Extreme Poses. To evaluate the impact of pose distribution on 3D human mesh recovery, we follow [54] that does not encode pose as a set of rotations. It is argued that the joint hierarchy and discontinuity of rotation representation make pose parameters θ of SMPL not straightforward. Hence, we represent each pose as a set of 3D coordinates of the 24 key joints in our evaluation, and plots the distribution of poses via PCA dimension reduction in Figure 3. Our study in Figure 5(c-d) indicates the importance of a large coverage of poses in the training set as model performance is again closely related to the data density. In addition, we plot the same results against pose distance from the distribution mean, and pose distance from the T-pose. We find out that T-pose, the neutral pose defined in SMPL is in fact not the actual center of all daily poses, validating the design convention to regress from a mean pose instead of the T-pose in regression-based methods.

Occlusions. With realistic physical interaction with the environment and camera placement, GTA-Human offers the

Table 5. **Big data and big model.** We extend our study from ResNet-50 to larger backbones, and find the trend consistent: using GTA-Human data always improve model performance by a large margin, regardless of the backbone. Note that the transformer for 3D human recovery is relatively less explored in the literature; the results may still have room for improvement. Nevertheless, the same trend holds on the two transformer baselines. #Param.: number of parameters. Real: training with only the real datasets. Blended: mix GTA-Human in the training. Values in green indicate the error reduction compared to the same models trained only on real data.

Backbone	#Param.	Real		Blended	
		MPJPE ↓	PA-MPJPE ↓	MPJPE ↓	PA-MPJPE ↓
ResNet-50	26M	98.5	61.7	88.7 (-9.8)	56.0 (-5.7)
ResNet-101	45M	94.8	60.1	86.7 (-8.1)	54.5 (-5.6)
ResNet-152	60M	89.8	58.4	87.6 (-2.2)	54.3 (-4.1)
DeiT-Small	22M	105.9	66.5	96.4 (-9.5)	60.7 (-5.8)
DeiT-Base	86M	94.0	61.2	91.1 (-2.9)	56.2 (-5.0)

Table 6. **Strong supervision is key.** We compare the effects of weak supervision (2D and 3D keypoints) with strong supervision (SMPL parameters) of GTA-Human, and discover that adding strong supervision is much more effective, and combining the two only gives marginal improvement on the primary metric PA-MPJPE on top of using the strong supervision alone. This does not only highlight the value of GTA-Human for having a mega-scale of SMPL annotations, but also suggest SMPL annotation may serve as the most critical annotation. The first row is the HMR baseline without any GTA-Human data added.

Keypoints	SMPL	MPJPE ↓	PA-MPJPE ↓
		98.5	61.7
✓		93.4	60.9
	✓	92.0	56.3
✓	✓	88.7	56.0

possibility for an in-depth investigation into occlusion and its effects on 3D human recovery. We show in Figure 5(e-f) that the increment in the percentage of body parts occluded (or self-occluded) leads to a rapid performance drop.

5. Conclusion

We present GTA-Human, a large-scale synthetic dataset that features high diversity and realisticness for both image- and video-based 3D human recovery. Our experiments on GTA-Human provide four major insights: **1)** Seemingly unreasonable improvements are achieved given a large amount of data is available, even without any domain adaptation techniques. **2)** The large amount of data is also effective on deeper and more powerful models to achieve consistent improvements. **3)** For human pose and shape estimation, strong supervision such as SMPL parameters are more effective, also essential, for training a high-performance model. **4)** We also identify that rare camera angles, severe occlusion, and extreme poses undermines estimation accuracy and studied their impacts closely. We discuss ethical concerns in the Sup-

plementary Material. For future work, there may exist some domain gaps between GTA-Human and real datasets, and it is very interesting to study the sim2real problem for human pose and shape estimation on GTA-Human. In addition, our findings for SMPL may be extended to SMPL-X, a more sophisticated human parametric model with the face and the hands. Furthermore, GTA-Human supports the study on novel modalities such as point clouds, providing alternative solutions to existing image- and video-based models.

References

- [1] Mykhaylo Andriluka, Leonid Pishchulin, Peter Gehler, and Bernt Schiele. 2d human pose estimation: New benchmark and state of the art analysis. In *Proceedings of the IEEE Conference on computer Vision and Pattern Recognition*, pages 3686–3693, 2014. [2](#), [12](#), [15](#)
- [2] Anurag Arnab, Carl Doersch, and Andrew Zisserman. Exploiting temporal context for 3d human pose estimation in the wild. In *Proceedings of the IEEE/CVF Conference on Computer Vision and Pattern Recognition*, pages 3395–3404, 2019. [7](#), [12](#)
- [3] Federica Bogo, Angjoo Kanazawa, Christoph Lassner, Peter Gehler, Javier Romero, and Michael J Black. Keep it smpl: Automatic estimation of 3d human pose and shape from a single image. In *European conference on computer vision*, pages 561–578. Springer, 2016. [12](#), [14](#), [17](#)
- [4] Zhongang Cai, Junzhe Zhang, Daxuan Ren, Cunjun Yu, Haiyu Zhao, Shuai Yi, Chai Kiat Yeo, and Chen Change Loy. Messytable: Instance association in multiple camera views. In *European Conference on Computer Vision*, pages 1–16. Springer, 2020. [4](#)
- [5] Zhe Cao, Hang Gao, Karttikeya Mangalam, Qi-Zhi Cai, Minh Vo, and Jitendra Malik. Long-term human motion prediction with scene context. In *European Conference on Computer Vision*, pages 387–404. Springer, 2020. [2](#), [3](#), [16](#)
- [6] Hongsuk Choi, Gyeongsik Moon, and Kyoung Mu Lee. Beyond static features for temporally consistent 3d human pose and shape from a video. In *Conference on Computer Vision and Pattern Recognition (CVPR)*, 2021. [12](#), [17](#)

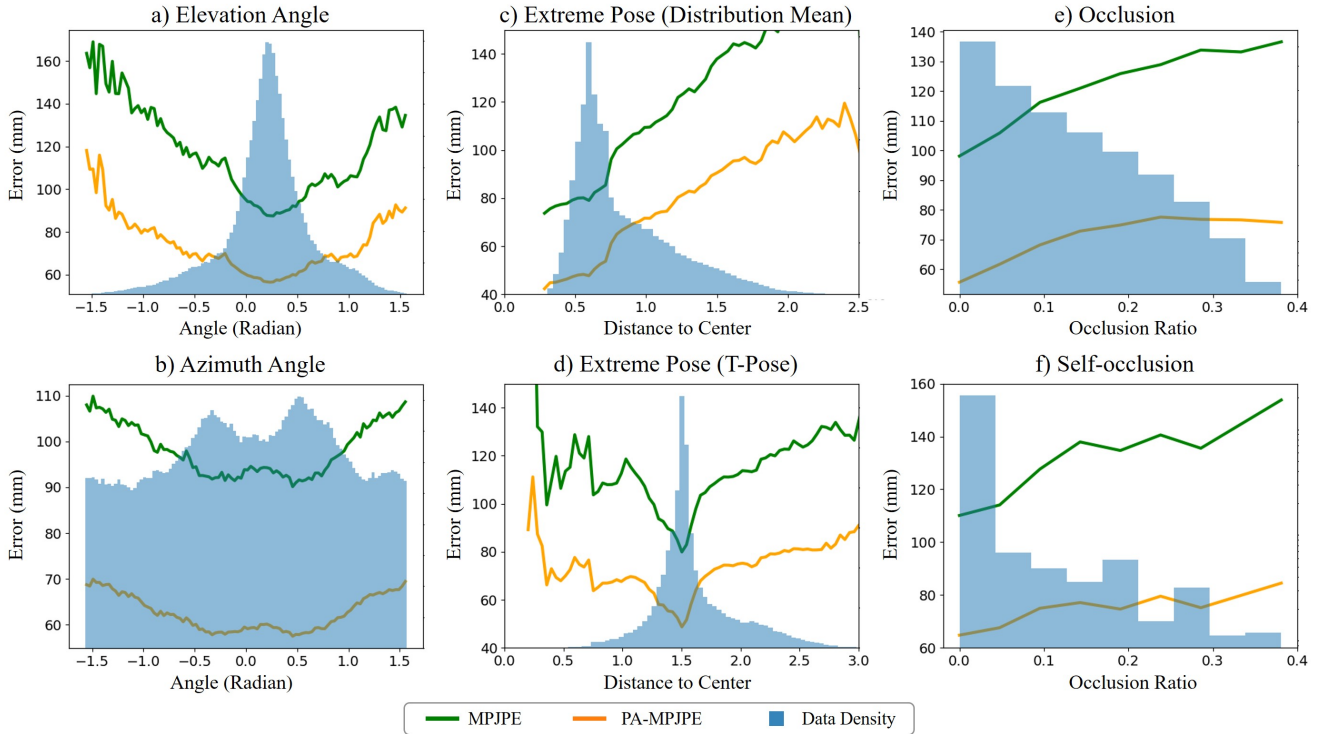


Figure 5. **Systematic study on real-world variations.** We identify three factors: **camera angles, extreme poses, and occlusions.** We plot model performance against (a) elevation angle; (b) azimuth angle; (c) pose distance to distribution mean; (d) pose distance to T-pose; (e) occlusion ratio; (f) self-occlusion ratio. All results suggest that the data imbalance leads to severe performance degradation at where the data is insufficient. We discretize all examples evaluated and plot the data density with bins, and compute the mean error for each bin to form the curves. More discussion is found in Section 4.5. The density of e) and f) is in log scale.

- [7] Carl Doersch and Andrew Zisserman. Sim2real transfer learning for 3d human pose estimation: motion to the rescue. In *NeurIPS*, pages 12929–12941, 2019. 15
- [8] Alexey Dosovitskiy, Lucas Beyer, Alexander Kolesnikov, Dirk Weissenborn, Xiaohua Zhai, Thomas Unterthiner, Mostafa Dehghani, Matthias Minderer, Georg Heigold, Sylvain Gelly, Jakob Uszkoreit, and Neil Houlsby. An image is worth 16x16 words: Transformers for image recognition at scale. In *ICLR*. OpenReview.net, 2021. 2
- [9] Matteo Fabbri, Fabio Lanzi, Simone Calderara, Andrea Palazzi, Roberto Vezzani, and Rita Cucchiara. Learning to detect and track visible and occluded body joints in a virtual world. In *Proceedings of the European Conference on Computer Vision (ECCV)*, pages 430–446, 2018. 2, 3, 13, 16
- [10] Georgios Georgakis, Ren Li, Srikrishna Karanam, Terrence Chen, Jana Košecká, and Ziyang Wu. Hierarchical kinematic human mesh recovery. In *European Conference on Computer Vision*, pages 768–784. Springer, 2020. 12
- [11] John C Gower. Generalized procrustes analysis. *Psychometrika*, 40(1):33–51, 1975. 5
- [12] Shanyan Guan, Jingwei Xu, Yunbo Wang, Bingbing Ni, and Xiaokang Yang. Bilevel online adaptation for out-of-domain human mesh reconstruction. In *CVPR*, pages 10472–10481. Computer Vision Foundation / IEEE, 2021. 15
- [13] Riza Alp Guler and Iasonas Kokkinos. Holopose: Holistic 3d human reconstruction in-the-wild. In *Proceedings of the IEEE/CVF Conference on Computer Vision and Pattern Recognition*, pages 10884–10894, 2019. 12
- [14] Kaiming He, Xiangyu Zhang, Shaoqing Ren, and Jian Sun. Deep residual learning for image recognition. In *Proceedings of the IEEE conference on computer vision and pattern recognition*, pages 770–778, 2016. 2, 6, 12
- [15] David T. Hoffmann, Dimitrios Tzionas, M. Black, and Siyu Tang. Learning to train with synthetic humans. In *GCPR*, 2019. 2
- [16] Yuan-Ting Hu, Jiahong Wang, Raymond A Yeh, and Alexander G Schwing. Sail-vos 3d: A synthetic dataset and baselines for object detection and 3d mesh reconstruction from video data. In *Proceedings of the IEEE/CVF Conference on Computer Vision and Pattern Recognition*, pages 1418–1428, 2021. 2, 3, 16
- [17] Yinghao Huang, Federica Bogo, Christoph Lassner, Angjoo Kanazawa, Peter V Gehler, Javier Romero, Ijaz Akhter, and Michael J Black. Towards accurate marker-less human shape and pose estimation over time. In *2017 international conference on 3D vision (3DV)*, pages 421–430. IEEE, 2017. 12
- [18] Catalin Ionescu, Dragos Papava, Vlad Olaru, and Cristian

- Sminchisescu. Human3.6m: Large scale datasets and predictive methods for 3d human sensing in natural environments. *IEEE transactions on pattern analysis and machine intelligence*, 36(7):1325–1339, 2013. 1, 2, 3, 4, 15
- [19] Sam Johnson and Mark Everingham. Clustered pose and nonlinear appearance models for human pose estimation. In *BMVC*, pages 1–11. British Machine Vision Association, 2010. 2, 12, 15
- [20] Sam Johnson and M. Everingham. Learning effective human pose estimation from inaccurate annotation. *CVPR 2011*, pages 1465–1472, 2011. 2, 12, 15
- [21] H. Joo, N. Neverova, and A. Vedaldi. Exemplar fine-tuning for 3d human pose fitting towards in-the-wild 3d human pose estimation. *ArXiv*, abs/2004.03686, 2020. 3, 7, 12
- [22] H. Joo, Tomas Simon, Xulong Li, H. Liu, L. Tan, Lin Gui, Sean Banerjee, Timothy Godisart, Bart C. Nabbe, I. Matthews, T. Kanade, S. Nobuhara, and Yaser Sheikh. Panoptic studio: A massively multiview system for social interaction capture. *IEEE Transactions on Pattern Analysis and Machine Intelligence*, 41:190–204, 2019. 1, 2, 3, 4
- [23] Angjoo Kanazawa, Michael J Black, David W Jacobs, and Jitendra Malik. End-to-end recovery of human shape and pose. In *Proceedings of the IEEE Conference on Computer Vision and Pattern Recognition*, pages 7122–7131, 2018. 2, 5, 6, 12, 15, 16, 17
- [24] Angjoo Kanazawa, Jason Y Zhang, Panna Felsen, and Jitendra Malik. Learning 3d human dynamics from video. In *Proceedings of the IEEE/CVF Conference on Computer Vision and Pattern Recognition*, pages 5614–5623, 2019. 12, 17
- [25] Imry Kissos, Lior Fritz, Matan Goldman, Omer Meir, Eduard Oks, and Mark Kliger. Beyond weak perspective for monocular 3d human pose estimation. In *European Conference on Computer Vision*, pages 541–554. Springer, 2020. 14, 16
- [26] Muhammed Kocabas, Nikos Athanasiou, and Michael J Black. Vibe: Video inference for human body pose and shape estimation. In *Proceedings of the IEEE/CVF Conference on Computer Vision and Pattern Recognition*, pages 5253–5263, 2020. 2, 5, 6, 7, 12, 15, 17
- [27] Muhammed Kocabas, Chun-Hao P Huang, Otmar Hilliges, and Michael J Black. Pare: Part attention regressor for 3d human body estimation. *arXiv preprint arXiv:2104.08527*, 2021. 12
- [28] Nikos Kolotouros, Georgios Pavlakos, Michael J Black, and Kostas Daniilidis. Learning to reconstruct 3d human pose and shape via model-fitting in the loop. In *Proceedings of the IEEE/CVF International Conference on Computer Vision*, pages 2252–2261, 2019. 2, 5, 6, 12, 15, 16, 17
- [29] Nikos Kolotouros, Georgios Pavlakos, and Kostas Daniilidis. Convolutional mesh regression for single-image human shape reconstruction. In *Proceedings of the IEEE/CVF Conference on Computer Vision and Pattern Recognition*, pages 4501–4510, 2019. 17
- [30] Philipp Krähenbühl. Free supervision from video games. In *Proceedings of the IEEE Conference on Computer Vision and Pattern Recognition*, pages 2955–2964, 2018. 2, 3, 14, 16
- [31] Jonathan Krause, Benjamin Sapp, Andrew Howard, Howard Zhou, Alexander Toshev, Tom Duerig, James Philbin, and Li Fei-Fei. The unreasonable effectiveness of noisy data for fine-grained recognition. In *European Conference on Computer Vision*, pages 301–320. Springer, 2016. 1
- [32] Christoph Lassner, Javier Romero, Martin Kiefel, Federica Bogo, Michael J Black, and Peter V Gehler. Unite the people: Closing the loop between 3d and 2d human representations. In *Proceedings of the IEEE conference on computer vision and pattern recognition*, pages 6050–6059, 2017. 12
- [33] Vincent Leroy, Philippe Weinzaepfel, Romain Bréger, Hadrien Combaluzier, and Grégory Rogez. Simply benchmarking 3d human pose estimation in the wild. *2020 International Conference on 3D Vision (3DV)*, pages 301–310, 2020. 1, 2, 3
- [34] Jiefeng Li, Chao Xu, Zhicun Chen, Siyuan Bian, Lixin Yang, and Cewu Lu. Hybrik: A hybrid analytical-neural inverse kinematics solution for 3d human pose and shape estimation. In *CVPR*, pages 3383–3393. Computer Vision Foundation / IEEE, 2021. 12
- [35] Kevin Lin, Lijuan Wang, and Zicheng Liu. End-to-end human pose and mesh reconstruction with transformers. In *CVPR*, pages 1954–1963. Computer Vision Foundation / IEEE, 2021. 12
- [36] Tsung-Yi Lin, Michael Maire, Serge Belongie, James Hays, Pietro Perona, Deva Ramanan, Piotr Dollár, and C Lawrence Zitnick. Microsoft coco: Common objects in context. In *European conference on computer vision*, pages 740–755. Springer, 2014. 2, 12, 15
- [37] Matthew Loper, Naureen Mahmood, and Michael J Black. Mosh: Motion and shape capture from sparse markers. *ACM Transactions on Graphics (TOG)*, 33(6):1–13, 2014. 5, 6, 7, 15
- [38] Matthew Loper, Naureen Mahmood, Javier Romero, Gerard Pons-Moll, and Michael J Black. SMPL: A skinned multi-person linear model. *ACM transactions on graphics (TOG)*, 34(6):1–16, 2015. 1, 12
- [39] Zhengyi Luo, S Alireza Golestaneh, and Kris M Kitani. 3d human motion estimation via motion compression and refinement. In *Proceedings of the Asian Conference on Computer Vision*, 2020. 12
- [40] Dushyant Mehta, Helge Rhodin, Dan Casas, Pascal Fua, Oleksandr Sotnychenko, Weipeng Xu, and Christian Theobalt. Monocular 3d human pose estimation in the wild using improved cnn supervision. In *2017 international conference on 3D vision (3DV)*, pages 506–516. IEEE, 2017. 2, 3, 4, 15
- [41] Dushyant Mehta, Oleksandr Sotnychenko, Franziska Mueller, Weipeng Xu, Mohamed Elgharib, Pascal Fua, Hans-Peter Seidel, Helge Rhodin, Gerard Pons-Moll, and Christian Theobalt. Xnect: Real-time multi-person 3d motion capture with a single rgb camera. *ACM Transactions on Graphics (TOG)*, 39(4):82–1, 2020. 12
- [42] Dushyant Mehta, Oleksandr Sotnychenko, F. Mueller, Weipeng Xu, Srinath Sridhar, Gerard Pons-Moll, and C. Theobalt. Single-shot multi-person 3d pose estimation from monocular rgb. *2018 International Conference on 3D Vision (3DV)*, pages 120–130, 2018. 2
- [43] Gyeongsik Moon and Kyoung Mu Lee. I2l-meshnet: Image-to-lixel prediction network for accurate 3d human pose and

- mesh estimation from a single RGB image. In *ECCV* (7), volume 12352 of *Lecture Notes in Computer Science*, pages 752–768. Springer, 2020. 12, 17
- [44] Mohamed Omran, Christoph Lassner, Gerard Pons-Moll, Peter Gehler, and Bernt Schiele. Neural body fitting: Unifying deep learning and model based human pose and shape estimation. In *2018 international conference on 3D vision (3DV)*, pages 484–494. IEEE, 2018. 12
- [45] Ahmed A. A. Osman, Timo Bolkart, and Michael J. Black. STAR: sparse trained articulated human body regressor. In *ECCV* (6), volume 12351 of *Lecture Notes in Computer Science*, pages 598–613. Springer, 2020. 12
- [46] Priyanka Patel, Chun-Hao P. Huang, Joachim Tesch, David T. Hoffmann, Shashank Tripathi, and Michael J. Black. AGORA: Avatars in geography optimized for regression analysis. In *Proceedings IEEE/CVF Conf. on Computer Vision and Pattern Recognition (CVPR)*, June 2021. 2, 3, 5, 6, 7
- [47] Georgios Pavlakos, Vasileios Choutas, Nima Ghorbani, Timo Bolkart, Ahmed AA Osman, Dimitrios Tzionas, and Michael J Black. Expressive body capture: 3d hands, face, and body from a single image. In *Proceedings of the IEEE/CVF Conference on Computer Vision and Pattern Recognition*, pages 10975–10985, 2019. 12
- [48] Georgios Pavlakos, Jitendra Malik, and Angjoo Kanazawa. Human mesh recovery from multiple shots. *arXiv preprint arXiv:2012.09843*, 2020. 17
- [49] Georgios Pavlakos, Luyang Zhu, Xiaowei Zhou, and Kostas Daniilidis. Learning to estimate 3d human pose and shape from a single color image. In *Proceedings of the IEEE Conference on Computer Vision and Pattern Recognition*, pages 459–468, 2018. 12
- [50] Albert Pumarola, Jordi Sanchez, G. Choi, A. Sanfeliu, and F. Moreno-Noguer. 3dpeople: Modeling the geometry of dressed humans. *2019 IEEE/CVF International Conference on Computer Vision (ICCV)*, pages 2242–2251, 2019. 2
- [51] Stephan R Richter, Zeeshan Hayder, and Vladlen Koltun. Playing for benchmarks. In *Proceedings of the IEEE International Conference on Computer Vision*, pages 2213–2222, 2017. 2, 3, 16
- [52] Stephan R Richter, Vibhav Vineet, Stefan Roth, and Vladlen Koltun. Playing for data: Ground truth from computer games. In *European conference on computer vision*, pages 102–118. Springer, 2016. 2, 3, 16
- [53] Yu Rong, Ziwei Liu, Cheng Li, Kaidi Cao, and Chen Change Loy. Delving deep into hybrid annotations for 3d human recovery in the wild. In *Proceedings of the IEEE/CVF International Conference on Computer Vision*, pages 5340–5348, 2019. 1
- [54] Yu Rong, Ziwei Liu, and Chen Change Loy. Chasing the tail in monocular 3d human reconstruction with prototype memory. *arXiv preprint arXiv:2012.14739*, 2020. 7
- [55] Akash Sengupta, Roberto Cipolla, and Ignas Budvytis. Synthetic training for accurate 3d human pose and shape estimation in the wild. In *BMVC*. BMVA Press, 2020. 12
- [56] L. Sigal, A. O. Balan, and Michael J. Black. Humaneva: Synchronized video and motion capture dataset and baseline algorithm for evaluation of articulated human motion. *International Journal of Computer Vision*, 87:4–27, 2009. 1, 2, 3, 4
- [57] Jie Song, Xu Chen, and Otmar Hilliges. Human body model fitting by learned gradient descent. In *ECCV* (20), volume 12365 of *Lecture Notes in Computer Science*, pages 744–760. Springer, 2020. 12, 17
- [58] Chen Sun, Abhinav Shrivastava, Saurabh Singh, and Abhinav Gupta. Revisiting unreasonable effectiveness of data in deep learning era. In *Proceedings of the IEEE international conference on computer vision*, pages 843–852, 2017. 1
- [59] Yu Sun, Yun Ye, Wu Liu, Wenpeng Gao, Yili Fu, and Tao Mei. Human mesh recovery from monocular images via a skeleton-disentangled representation. In *Proceedings of the IEEE/CVF International Conference on Computer Vision*, pages 5349–5358, 2019. 12, 17
- [60] Hugo Touvron, Matthieu Cord, Matthijs Douze, Francisco Massa, Alexandre Sablayrolles, and Hervé Jégou. Training data-efficient image transformers & distillation through attention. In *ICML*, volume 139 of *Proceedings of Machine Learning Research*, pages 10347–10357. PMLR, 2021. 2, 6
- [61] Matthew Trumble, Andrew Gilbert, Charles Malleon, A. Hilton, and J. Collomosse. Total capture: 3d human pose estimation fusing video and inertial sensors. In *BMVC*, 2017. 2
- [62] Gül Varol, J. Romero, Xavier Martin, Naureen Mahmood, Michael J. Black, I. Laptev, and C. Schmid. Learning from synthetic humans. *2017 IEEE Conference on Computer Vision and Pattern Recognition (CVPR)*, pages 4627–4635, 2017. 2, 3
- [63] Timo von Marcard, Roberto Henschel, Michael J Black, Bodo Rosenhahn, and Gerard Pons-Moll. Recovering accurate 3d human pose in the wild using imus and a moving camera. In *Proceedings of the European Conference on Computer Vision (ECCV)*, pages 601–617, 2018. 1, 2, 3, 5, 6, 7, 15, 17
- [64] Saining Xie, Ross Girshick, Piotr Dollár, Zhuowen Tu, and Kaiming He. Aggregated residual transformations for deep neural networks. In *Proceedings of the IEEE conference on computer vision and pattern recognition*, pages 1492–1500, 2017. 2
- [65] Zhixuan Yu, J. S. Yoon, I. Lee, Prashanth Venkatesh, Jaesik Park, J. Yu, and H. Park. Humbi: A large multiview dataset of human body expressions. *2020 IEEE/CVF Conference on Computer Vision and Pattern Recognition (CVPR)*, pages 2987–2997, 2020. 1, 2
- [66] Tianshu Zhang, Buzhen Huang, and Yangang Wang. Object-occluded human shape and pose estimation from a single color image. *2020 IEEE/CVF Conference on Computer Vision and Pattern Recognition (CVPR)*, pages 7374–7383, 2020. 12

A. Additional Related Works

A.1. Datasets with 2D Keypoint Annotations

There are many datasets that contain in-the-wild images, albeit the lack of SMPL annotations, they provide 2D keypoint labels. Datasets such as LSP [19], LSP-Extended [20], COCO [36] and MPII [1] contain images crawled from the Internet, and are annotated with 2D keypoints manually. Such a strategy allows a large number of in-the-wild images to be included in the dataset. To obtain 3D annotations that are crucial to human pose and shape estimation, a common method is to fit an SMPL model on 2D keypoints. SSP-3D [55] and 3DOH50K [66] leverages pre-trained model to perform keypoint estimation as the first step, whereas UP-3D [32] and EFT [21] performs fitting on ground truth keypoints. However, these datasets typically suffer from the inherent depth ambiguity of images and the pseudo-SMPL may not have the accurate scale.

A.2. 3D Human Recovery Methods

Human Parametric Models. 3D human recovery is usually performed on 3D human parametric models, such as SMPL [38], SMPL-X [47] and STAR [45], which take in parameters that represent pose and shape of the human subject, and output 3D human mesh via linear blend skinning. We base our discussion on SMPL version 1.0 in this work that consists of pose parameters $\theta \in \mathbb{R}^{72}$ and shape parameters $\beta \in \mathbb{R}^{10}$, for its popularity.

Optimization-based Methods. As the output of the human parametric model is manipulated by body parameters, SMPLify [3] and the following SMPLify-X [47] are the pioneering works to optimize these parameters to minimize the distance between ground truth 2D keypoints and reprojected human mesh joints. SMPLify is also extended to videos with temporal constraints employed [17]. Although optimization-based methods are able to achieve impressive results, they are slow and typically take more than 60 seconds per frame.

Regression-based Methods. Direct regression of body parameters using a trained deep learning model has gained more popularity due to fast inference. The recent works are categorized into image-based [10, 13, 27, 44, 49], and video-based [6, 24, 39, 41, 43, 59] methods. HMR [23] is a pioneering end-to-end deep learning-based work, which takes ResNet-50 [14] as its backbone and directly regress the parameters of θ and β . VIBE [26] is a milestone video-based work that leverages temporal information for realistic pose sequences. Recently, a transformer encoder is introduced for vertex-joint reweighting [35], but the method still relies on the CNN backbone for feature extraction.

Mixed Methods. There is a line of work that combines optimization-based and regression-based techniques. SPIN [28], adds a SMPLify step to produce pseudo parametric labels to guide the learning of the network. SPIN

address the lack of SMPL annotation but the optimization step results in slow training. Others propose to refine the per-frame regression results by bundle adjustment of the video sequence as a whole [2], designing a new swing-twist representation to replace the original axis-angle representation of SMPL [34], leveraging a trained network and finetune the network to obtain refined prediction [21], and employing a network to predict a parameter update rule in iterations of optimization [57].

B. Additional Details of GTA-Human

More examples in GTA-Human are found in Figure 6.

B.1. Toolchain

We develop a customized toolchain to automatically collect and annotate data from the game GTA-V. Note that to achieve scalability and efficiency, we leverage cloud-based services for parallel deployment of our tools on multiple computer instances and GPU cluster nodes. The toolchain is illustrated in Figure 7.

- **Cloud-based NoSQL Database.** The unit of data in GTA-Human is a single video sequence. Hence, we employ a Database that is hosted on the cloud, to track the progress of data generation and processing of each sequence. The status of a sequence is updated at each stage in the toolchain, which we elaborate on in details below.
- **Scenario File Generator.** This tool reads from the Database to retrieve sequence IDs that are either not generated before or failed in previous processing attempts, and produce random scene attributes such as subject ID, action ID, location in the 3D virtual world, camera position and orientation, lighting, and weather settings.
- **Cloud-based Message FIFO Queue.** The Message FIFO Queue parse the scenario files from the Scenario File Generator as text strings, which can be fetched in the first-in-first-out (FIFO) manner by multiple Local GUI Workers. Note that the queue allows for multiple workers to retrieve their next jobs simultaneously.
- **Local GUI Workers.** We purchase multiple copies of GTA-V and install them on regular gaming desktops. We refer to these desktops as Local GUI Workers. Each worker runs three tools: Scenario Controller, Data Collector, and Data Analyser that we elaborate on below.
- **Scenario Controller.** Taking scenario files as the input, Scenario Controller is essentially a plugin that interacts with the game engine via the designated Application Programming Interface (API). It is thus able to control the subject generation and placement, action assignment to the subject, camera placement, in-game time, and weather.

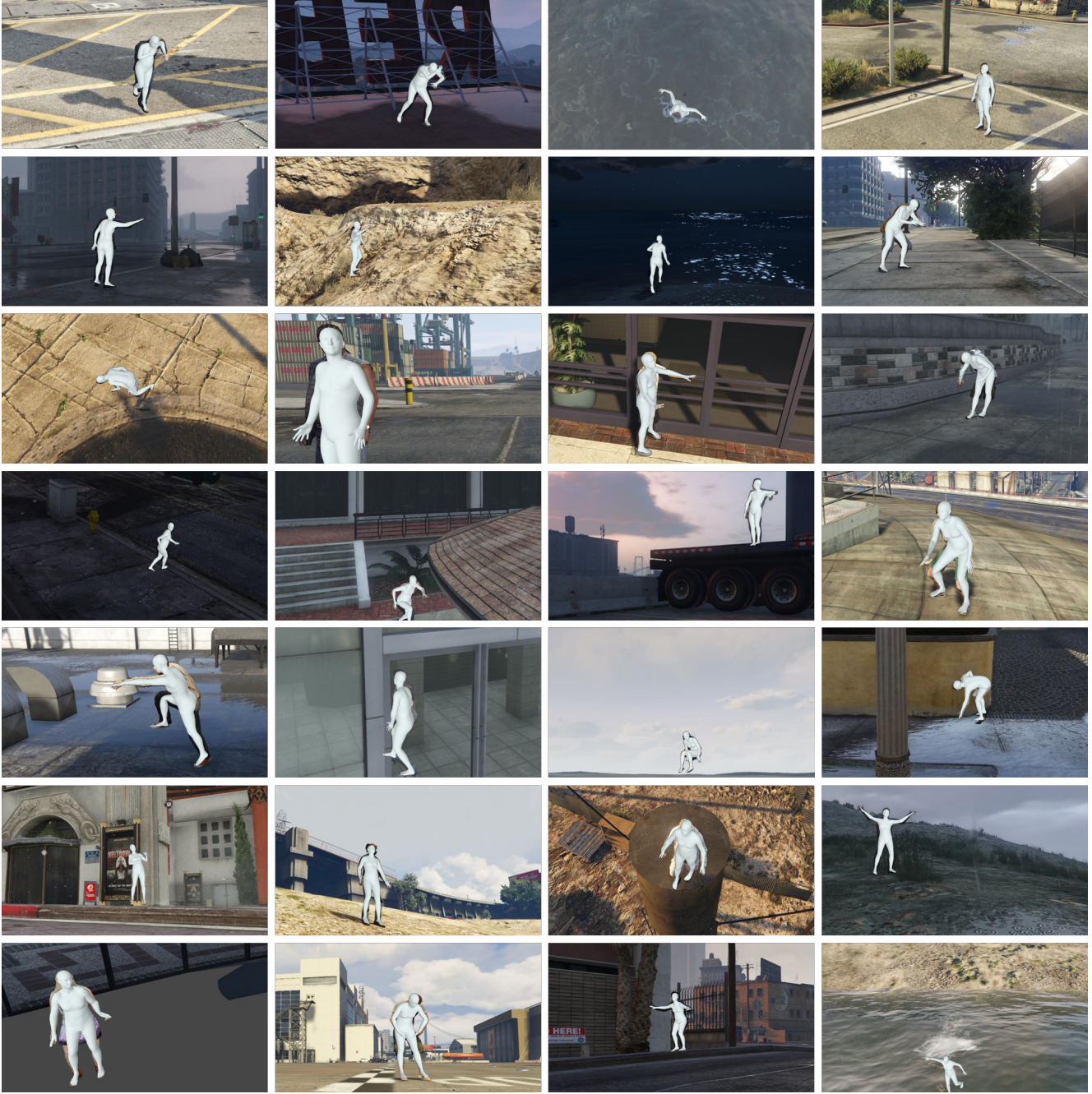


Figure 6. **More examples of GTA-Human.** We highlight that GTA-Human is a large-scale, highly diverse (in terms of subject appearances, actions and locations) datasets. Each frame of the video clips is annotated with SMPL parameters.

- **Data Collector.** This tool obtains data and some annotations from the API provided by GTA-V. First, it extracts 3D keypoints from each subject via the API provided by GTA-V. In addition to the original 98 keypoints available, we further obtain head top [9] and nose from interpolation of existing keypoints. We project 3D keypoints to the image plane with known intrinsic and extrinsic parame-

ters of the camera to obtain 2D keypoints. Second, we project light rays at each joint to determine if the joint is occluded or self-occluded by checking the entity that the light ray hits first [9]. Third, our tool intercepts the rendering pipeline, powered by DirectX, for depth maps and semantic masks. The pixel-wise depth is directly read from depth buffers. Shader injection enables the segmen-

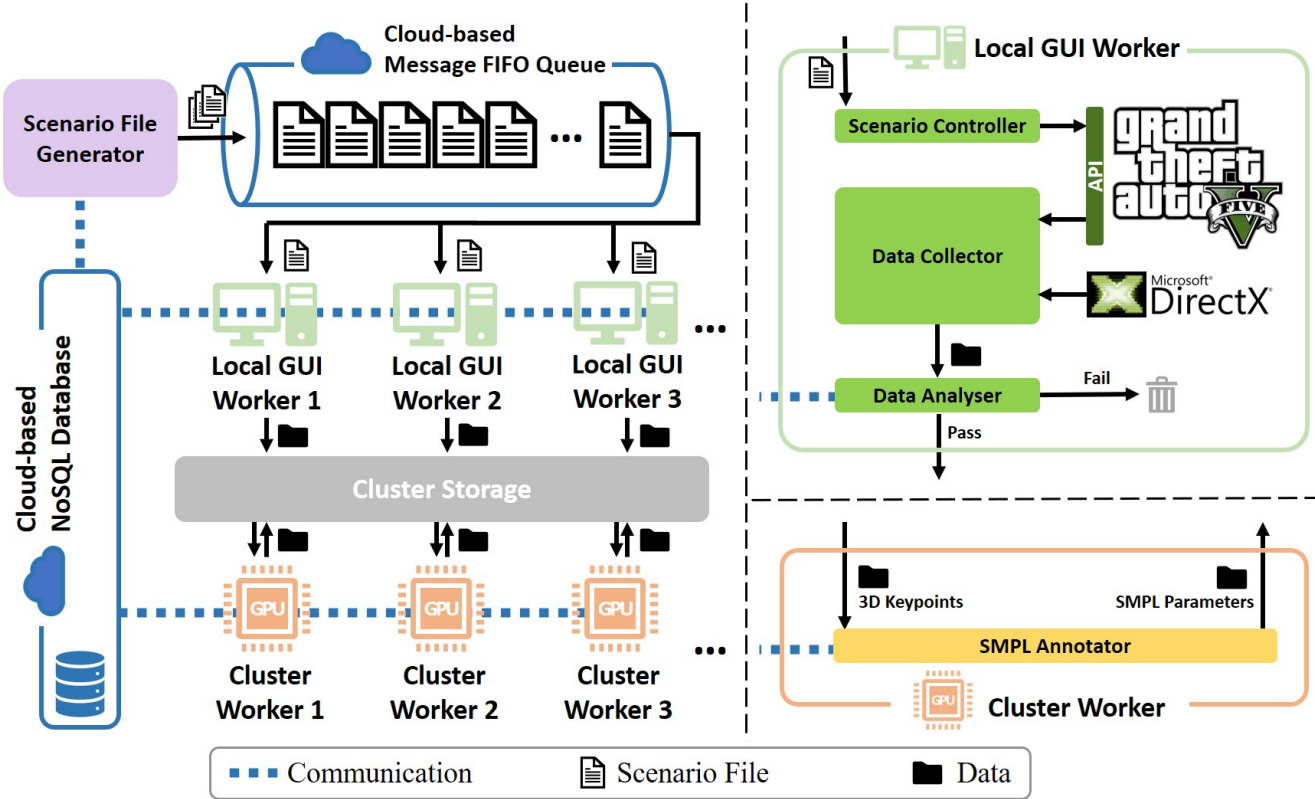


Figure 7. **Toolchain.** Left: the overview of the pipeline. Top right: an elaborate illustration of Local GUI Worker. Bottom right: an elaborate illustration of Cluster Worker. Our toolchain is highly scalable as the cloud-based services are used to coordinate a large number of workers.

tation of individual patches, and we manually assign the semantic class to various shaders based on their variable names. We refer interested readers to [30] for more details. Fourth, the collector also records videos.

- **Data Analyser.** To filter out low-quality data in the early stage, Data Analyser imposes several constraints on 3D keypoints obtained. We compute joint movement speed simply as the position different in consecutive frames to filter out less expressive actions (slow-moving or stationary actions). Severely occluded, or out-of-view subjects are also flagged at this stage. If sequences pass the analysis, their data are transferred from the local storage to a centralized storage space on our GPU cluster (Cluster Storage) for further processing. The failed ones, however, are deleted. The Database is notified of the result to get the status updated.
- **Cluster Workers and SMPL Annotator.** On each Cluster Worker (a GPU in the cluster), we run an instance of SMPL Annotator that takes keypoint annotation from the Cluster Storage. We upgrade SMPLify [3] in two ways to obtain accurate SMPL annotation. 1) we find out that compared to 2D keypoints that have inherent depth ambiguity,

exacerbated by weak perspective projection [25], 3D keypoints are unambiguous. Minor modifications are needed to replace the 2D keypoint loss of the original SMPLify with 3D keypoint loss. 2) Taking advantage of the fact that GTA-Human consists of video sequences instead of unrelated images, temporal consistency in the form of rotation smoothing and unified shape parameters are enforced. The SMPL parameters include θ and β , and an additional translation vector, are optimized at average one second per frame. We visualize more examples in GTA-Human that are produced with our SMPL annotation tool in Figure 6.

B.2. Camera Angle Distribution

Our data collection tool enables the control of camera placement position and orientation, thus allowing the study on camera angles that is otherwise difficult in real life. We visualize the camera angles in Figure 8.

B.3. GTA-Human as a Comprehensive Benchmark

Besides serving as an effective training source, GTA-Human may also be used as a challenging and indicative benchmark in comparison to other datasets in Table 7.

- **Challenging.** Methods that achieve satisfying results on

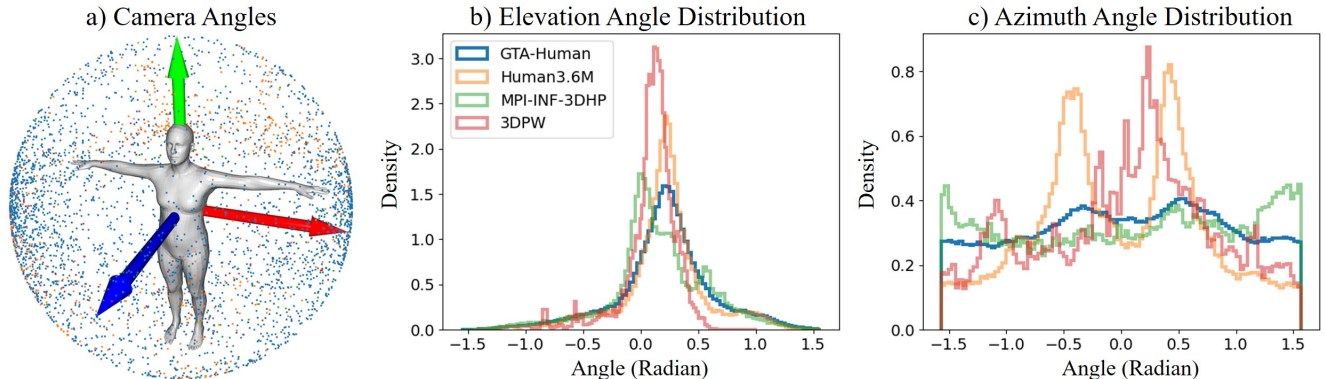


Figure 8. **Camera angles.** To balance diversity and realism, GTA-Human randomly generates virtual camera orientations by sampling azimuth and elevations values from the camera angle distributions of the real datasets. (a) Visualization of camera angles sampled from various datasets, normalized to a unit sphere. It is observed that GTA-Human provides a wide range of camera placements around the subject. The red, green, and blue arrows indicate X-, Y-, Z-axis respectively. (b) Elevation angle (up-down, with positive value indicating a camera placed higher than the waist and looking down) distributions. (c) Azimuth angle (around the subject on a horizontal plane) distributions. The colors of the points in (a) and line plots in (b) and (c) represent various datasets, shown in the legend in (b). Note the vertical axes of (b) and (c) represent data density, with area under the curve normalized to 1; GTA-Human has a much larger absolute scale if not normalized.

Table 7. **GTA-Human as a challenging and indicative benchmark.** We evaluate state-of-the-art (SOTA) methods on GTA-Human and compare the results with other standard benchmarks. GTA-Human has two ideal traits as a benchmark: it is 1) *challenging*: methods that perform well on other benchmarks give larger errors on GTA-Human; 2) *indicative*: methods that perform relatively well on GTA-Human also perform relatively well on other benchmarks. PA: PA-MPJPE. +: strong baseline of HMR, see Section 4.1. Note that we report evaluation results on the test split of GTA-Human. More details are included in the Supplementary Material.

Method	Human3.6M [18]		MPI-INF-3DHP [40]		3DPW [63]		GTA-Human	
	MPJPE ↓	PA ↓	MPJPE ↓	PA ↓	MPJPE ↓	PA ↓	MPJPE ↓	PA ↓
HMR [23]+	77.9	55.8	107.2	74.1	98.5	61.7	186.8	94.7
SPIN [28]	65.5	44.5	103.7	67.8	96.9	59.2	184.3	92.1
VIBE [26]	65.9	41.5	97.7	63.4	93.5	56.5	166.6	89.5

Human3.6M, MPI-INF-3DHP and 3DPW are still far from saturating on GTA-Human. Besides the large scale and wide variety of data included in the GTA-Human, domain gap is likely another significant factor. Hence, the research community may find GTA-Human useful for sim2real adaptation.

- **Indicative.** Methods that perform better on GTA-Human also have better performance on other popular datasets. The consistent trend observed may indicate that GTA-Human can serve as an indicative touchstone for method efficacy evaluation.

C. Additional Experiment Details

C.1. Datasets

We follow the convention of SPIN [28] and define the “Real” datasets used in the experiments include Human3.6M [18] (with SMPL annotations via MoSh [37]), MPI-INF-3DHP [40], LSP [19], LSP-Extended [20], MPII [1] and

COCO [36]. “Real” datasets consist of approximately 300K frames. “Blended” datasets are formed by simply mixing GTA-Human data with the “Real” data, note that no dataset weights or domain adaptation techniques [7, 12] are required.

C.2. Training Details

For HMR+, we remove all adversarial modules from the original HMR [23] for fast training. For the blended training, since GTA-Human has a much larger scale than existing datasets, we run all our experiments on 32 V100 GPUs, with the batch size of 2048 (four times as SPIN [28]). The learning rate is also scaled linearly by four times to 0.0002. The rest of the hyperparameters are the same as SPIN [28]. For the finetuning experiments, we use the learning rate of 0.00001 with the batch size of 512, on 8 V100 GPUs for two epochs.

D. Additional Discussions

D.1. Extended Comparison for the Unreasonable Effectiveness of Data

In Table 8, we extend our experiment results in the main paper and compare our models that leverage GTA-Human with recent works on human pose and shape estimation. We highlight that the GTA-Human is a large-scale, diverse, and well-annotated dataset; inclusion of GTA-Human allows HMR [23], a relatively simple baseline, to outperform more sophisticated works, some of which even leverages an optimization component or temporal information, without any modifications to the method.

D.2. On the Effectiveness of Strong Supervision

We elaborate more on the type of supervision signals and their effectiveness for human pose and shape estimation. Strong supervision in the form of ground truth SMPL parameters is directly used in the loss computation with the predicted SMPL parameters (Equation 1), which initiates gradient flow that reaches the learnable SMPL parameters in the shortest possible route. On the contrary, the 3D keypoints \hat{X}_{3D} are obtained after the linear blending skinning of the SMPL model \mathcal{M} and joint regression \mathcal{J} (Equation 2). The 2D keypoints \hat{X}_{2D} further require extra estimation of camera rotation \hat{R}_{cam} and translation $\hat{\mathbf{t}}_{cam}$ for the transformation \mathcal{T} of the 3D keypoints, and 3D to 2D projection \mathcal{K} with assumed focal length \mathbf{f} as well as camera center \mathbf{c} . The convoluted route and uncertainties introduced in the process to compute the loss for 2D keypoints (Equation 3) may be responsible for the ineffectiveness of weak supervision.

$$\mathcal{L}_{SMPL} = \|\theta - \hat{\theta}\| + \|\beta - \hat{\beta}\| \quad (1)$$

$$\mathcal{L}_{3D} = \|\hat{X}_{3D} - X_{3D}\| \quad (2)$$

$$\mathcal{L}_{2D} = \|\hat{X}_{2D} - X_{2D}\| \quad (3)$$

where

$$\hat{X}_{3D} = J(\mathcal{M}(\hat{\theta}, \hat{\beta})) \quad (4)$$

$$\hat{X}_{2D} = \mathcal{K}(\mathcal{T}(\hat{X}_{3D}, \hat{R}_{cam}, \hat{\mathbf{t}}_{cam}), \mathbf{f}, \mathbf{c}) \quad (5)$$

Our findings are in line with SPIN [28]. SPIN tests fitting 3D SMPL on 2D keypoints to produce pseudo SMPL annotations during training and finds this strategy effective. However, this conclusion still leaves the root cause of the effectiveness of 3D SMPL unanswered as recent work suggests that 2D supervision is inherently ambiguous [25]. In this work, we add in 3D keypoints as a better part of the weak supervision and find out that SMPL annotation is still far more effective. Hence, our work extends the study of SPIN and achieves a more in-depth conclusion that strong

supervision (SMPL parameters) is more effective than weak supervision (keypoints).

Besides, from a practical point of view, training with online optimization in SPIN is relatively slow and takes a lot of memory to store the temporary fitting results. In contrast, adding more data is well supported by fast data parallelism, implemented in modern deep learning frameworks.

E. Ethical Issues

E.1. Copyright

The game publisher allows for the use of game-generated materials as long as it is for non-commercial use, and no spoilers are distributed.¹² Hence, we follow prior works that generate data on the GTA game engine [5, 9, 16, 30, 51, 52] to make GTA-Human publically available.

E.2. Stereotypes and Biases

As we are aware of the biases embedded GTA (*e.g.* explicit content such as sexualized characters and violence), we work towards utilizing the dataset to the fullest for its academic values, at the same time uncovering and avoiding ethical issues. We adopt the following strategies in the data generation To minimize potential biases.

- All factors including the characters and actions, are decoupled, and randomized in GTA-Human. Specifically, the examples in GTA-Human are not linked to the original storylines; all the characters and the actions are pulled out of the in-game database, randomly assigned at random locations all over the map. Hence, it is very unlikely any character-specific actions could be reproduced. Moreover, no weapon is depicted in the datasets.
- We have conducted a manual analysis on clothing vs gender. As we find it difficult to determine if a specific attire has certain social implications without context (for example, skin-showing attire not be associated with sex workers as it is also common to find people in bikinis at the beach), we thus categorize all clothing into formal, semi-formal and casual. We observe that while there is approximately the same number of men and women in formal attires (11% vs 9%); more men in casual attires (*e.g.* tank tops, topless) than women (25% vs 11%). Hence, we find the character appearances mostly (albeit not perfectly) balanced across genders.
- We empirically find that the vast majority of the actions are used to depict the ordinary lives of the city-dwellers (*e.g.* walking, drinking coffee, doing push-ups, and so

¹Rockstar Games. PC single-player mods. <http://tinyurl.com/yc8kq7vn>

²Rockstar Games. Policy on posting copyrighted Rockstar Games material. <http://tinyurl.com/pjfoqo5>

Table 8. **More results on the unreasonable effectiveness of data.** We highlight that GTA-Human enables a relatively simple HMR baseline to outperform a series of newer works, some of which even employs more sophisticated strategies such as an optimization step (Opt) or temporal information (Video). HMR+ is a strong baseline that we train with our code for a fair comparison. Evaluation is conducted on 3DPW [63] test set, without using any 3DPW data in the train set.

Method	Year	Opt	Video	MPJPE ↓	PA-MPJPE ↓
SMPLify [3]	2016	✓	-	-	106.1
HMR [23]	2018	-	-	130.0	76.7
Kanazawa <i>et al.</i> [24]	2019	-	✓	116.5	72.6
GraphCMR [29]	2019	-	-	-	70.2
DSD+SATN [59]	2019	-	✓	-	69.5
SPIN [28]	2019	✓	-	96.9	59.2
I2L-MeshNet [43]	2020	-	✓	93.2	58.6
Pavlakos <i>et al.</i> [48]	2020	-	✓	-	57.8
VIBE [26]	2020	-	✓	93.5	56.5
Song <i>et al.</i> [57]	2020	✓	-	-	55.9
TCMR [6]	2021	-	✓	95.0	55.8
HMR+	2021	-	-	98.5	61.7
HMR-Mix	2021	-	-	88.7	56.0
HMR-FT	2021	-	-	87.0	52.7

on. This is further supported by 1) our analysis of action distribution in Figure 3, the distribution of GTA-Human is center-aligned with real datasets. 2) methods trained on GTA-Human can perform convincingly better on standard real datasets. Both indicate that the domain shift in actions may not severely be affected by the small portion of explicit actions.

- As much as we hope to perform a complete and thorough data screening and cleaning, we highlight it is not trivial to manually inspect all examples due to the sheer scale of the dataset. Hence, we anonymize the characters, actions, and locations such that they exist in the dataset to enrich the distribution, but cannot be retrieved for malicious uses.